Loss of *Tbx3* in Mouse Eye Causes Retinal Angiogenesis Defects Reminiscent of Human Disease

Mark L. Derbyshire,[1,2] Sruti Akula,[1,2] Austin Wong,[1,2] Karisa Rawlins,[1] Evelyn B. Voura,[1] William J. Brunken,[1] Michael E. Zuber,[1] Sabine Fuhrmann,[3] Anne M. Moon,[4–6] and Andrea S. Viczian[1]

[1]Ophthalmology and Visual Sciences Department, Upstate Medical University, Syracuse, New York, United States
[2]College of Medicine, Upstate Medical University, Syracuse, New York, United States
[3]Ophthalmology and Visual Sciences Department, Vanderbilt Eye Institute, Vanderbilt University, Nashville, Tennessee, United States
[4]Department of Molecular and Functional Genomics, Weis Center for Research, Geisinger Clinic, Danville, Pennsylvania, United States
[5]Department of Human Genetics, University of Utah, Salt Lake City, Utah, United States
[6]The Mindich Child Health and Development Institute, Hess Center for Science and Medicine at Mount Sinai, New York, New York, United States

Correspondence: Andrea S. Viczian, Ophthalmology and Visual Sciences Department, Upstate Medical University, 750 East Adams Street, Syracuse, NY 13210, USA; vicziana@upstate.edu.

MLD and SA contributed equally to the work presented here and should therefore be regarded as equivalent authors.

Received: July 5, 2022
Accepted: March 7, 2023
Published: May 1, 2023

Citation: Derbyshire ML, Akula S, Wong A, et al. Loss of *tbx3* in mouse eye causes retinal angiogenesis defects reminiscent of human disease. *Invest Ophthalmol Vis Sci.* 2023;64(5):1. https://doi.org/10.1167/iovs.64.5.1

Purpose. Familial exudative vitreoretinopathy (FEVR) and Norrie disease are examples of genetic disorders in which the retinal vasculature fails to fully form (hypovascular), leading to congenital blindness. While studying the role of a factor expressed during retinal development, T-box factor *Tbx3*, we discovered that optic cup loss of *Tbx3* caused the retina to become hypovascular. The purpose of this study was to characterize how loss of *Tbx3* affects retinal vasculature formation.

Methods. Conditional removal of *Tbx3* from both retinal progenitors and astrocytes was done using the optic cup-Cre recombinase driver *BAC-Dkk3-Cre* and was analyzed using standard immunohistochemical techniques.

Results. With *Tbx3* loss, the retinas were hypovascular, as seen in patients with retinopathy of prematurity (ROP) and FEVR. Retinal vasculature failed to form the stereotypic tri-layered plexus in the dorsal–temporal region. Astrocyte precursors were reduced in number and failed to form a lattice at the dorsal–temporal edge. We next examined retinal ganglion cells, as they have been shown to play a critical role in retinal angiogenesis. We found that melanopsin expression and Islet1/2-positive retinal ganglion cells were reduced in the dorsal half of the retina. In previous studies, the loss of melanopsin has been linked to hyaloid vessel persistence, which we also observed in the *Tbx3* conditional knockout (cKO) retinas, as well as in infants with ROP or FEVR.

Conclusions. To the best of our knowledge, these studies are the first demonstration that *Tbx3* is required for normal mammalian eye formation. Together, the results provide a potential genetic model for retinal hypovascular diseases.

Keywords: retinopathy of prematurity, angiogenesis, conditional knockout, *Tbx3*, retinal ganglion cells

Retinal development requires the synchronized formation of neural and vascular tissue for visual function. The early mouse retina remains avascular until differentiation of retinal cells causes an increase in metabolic demand. The differentiated cells release proteins that stimulate the migration and proliferation of astrocytes from the optic nerve just prior to birth.[1–3] Astrocyte precursors cling onto the axons of retinal ganglion cells (RGCs) as they migrate into the retina.[4,5] Migrating astrocyte precursors then produce signals to attract endothelial cells into the retina, which, in turn, produces proteins that cause the astrocytes to differentiate. Therefore, coordinated activity of neural, astrocyte, and endothelial cells is essential for nascent blood vessels to form a steady retinal blood supply. Disruption of signals from either the vascular cells or neurons halts retinal angiogenesis, creating a hypovascular retina seen in retinopathy of prematurity (ROP) and familial exudative vitreoretinopathy (FEVR).[1] Mutations in Wnt signaling pathway components, such as the Wnt receptor Frizzled4, are linked to these syndromes[6–9] and are responsible for 50% of FEVR cases.[1] The genetic mutations causing the remaining half of the FEVR cases are unknown.[1]

The signals that drive creation of the retinal vasculature function in concert with other signals that cause regression of the vascular source during embryonic development, the hyaloid artery. The hyaloid artery and its branches are a tran-

sient developmental vascular structure in many vertebrates. Regression of the hyaloid artery and its vessels is triggered by signals from intrinsically photosensitive retinal ganglion cells (ipRGCs).[10,11] Failure of the hyaloid vessels to regress leads to persistent fetal vasculature, which leads to intraocular hemorrhage and impairment of vision. Despite decades of study and its importance to human disease, a complete understanding the molecular regulation of retinal vascular development is still lacking.

In this study, we have identified a key factor, *Tbx3*, in cell types affecting retinal vascular development. In the frog (*Xenopus laevis*), *tbx3* is expressed in the eye field prior to optic vesicle formation where it plays an essential role early in eye formation.[12–16] Later in ocular development, *Tbx3* is found in the dorsal half of the optic cup in frogs, mice, and humans.[13,14,16–18] Functional studies of the role of *Tbx3* in mammalian eye formation have not been done. A study of the initial gene deletion of murine *Tbx3* did not study the eye[19] and found only a hypomorphic deletion.[20] A conditional ablation strategy was developed[20,21] and used successfully to study the role of *Tbx3* in several other tissues, including vascular cells during kidney development.[22–28]

We used a similar approach and investigated the role of *Tbx3* in mammalian retinal development with a combination of expression studies and reverse genetics to probe function. To our surprise, we found that *Tbx3* is expressed not only in embryonic retinal progenitors but also postnatally in retinal astrocyte precursors, amacrine, and ganglion cells in the newborn retina. To investigate the effect of *Tbx3* loss of function on retinal development, we crossed mice bearing the *Tbx3* conditional allele[20] with a Cre driver, *BAC-Dkk3-Cre*, that functions in retinal progenitors and astrocytes but not endothelial cells.[29,30] In the *Tbx3* conditional knockout (cKO) mice, we observed that the hyaloid vessels persisted, and the retina was hypovascular. We found fewer astrocytes in the dorsal *Tbx3* cKO retina at P2 and P9, and by P30 the astrocytic lattice was malformed in the dorsal retina. With *Tbx3* loss, we also found thinner optic nerves and fewer intrinsically photosensitive RGCs at birth. Together, these results suggest that *Tbx3* is required for mammalian eye formation and that this cKO could potentially be a new mouse model for hypovascular diseases.

Methods

Mice

Transgenic mouse strains, including BAC-Dickkopf3-Cre (*BAC-Dkk3-Cre*),[29] *Tie2-Cre*,[31,32] *ROSA26-LacZ*, *tbx3*^{mcm} (inducible Cre recombinase knocked into the *Tbx3* locus),[24] *Tbx3*-floxed, and *tbx3*^{GR},[20,21] were maintained on a C57Bl/6J background. Tamoxifen treatment was administered as previously described.[33] Briefly, inducible *tbx3*^{mcm} mice have two copies of the murine estrogen receptor flanking Cre recombinase knocked into the *Tbx3* gene locus.[24] Timed pregnancies were generated by crossing *tbx3*^{mcm} with *ROSA26-LacZ*. The dams were given 0.1 mg/g body weight of tamoxifen (T5648; Sigma-Aldrich, St. Louis, MO, USA) by oral gavage, when embryos had developed to E8.5, and they were then collected at E10.5 and E11.5 for LacZ staining. Cre activity was also assessed using the Ai9 Cre reporter line (B6.Cg-*Gt(ROSA)26Sor*$^{tm9(CAG\text{-}tdTomato)Hze}$/J, 007909; The Jackson Laboratory, Bar Harbor, ME, USA). We used sibling cKO (*BAC-Dkk3-Cre*$^{+}$;*tbx3*$^{\Delta Fl/\Delta Fl}$) and wild-type (*BAC-Dkk3-Cre*-negative;*tbx3*$^{Fl/+}$) mice (Supplementary Figs. S1A–S1F). At least two litters were used for analysis with the number of mice (*N*) indicated in the figures. We observed no difference in levels of TBX3 protein in male and female samples by western blot (Supplementary Fig. S1D); thus, we performed our analysis on a random mixture of sexes. This study was approved by the Upstate Institutional Animal Care and Use Committee and adhered to the ARVO Statement for the Use of Animals in Ophthalmic and Vision Research.

Genotyping

Ear punches or tail snips (1–2 mm) were incubated overnight at 55°C in 100 µL lysis buffer (10-mM Tris, pH 8.0; 100-mM NaCl; 10-mM EDTA, pH 8.0; 0.05% SDS) and 80 µg Proteinase K (20 mg/mL stock, P2308; Sigma-Aldrich). Samples were spun down at 14,000*g* for 15 minutes, 70-µL supernatant was placed in 200 µL ice-cold isopropanol, and the DNA was pelleted at 4°C and 14,000*g* for 10 minutes. This was followed by washing the samples twice with 70% ethanol, followed by drying and resuspension in 10-mM Tris, pH 8.0. PCR was performed as described in Supplementary Table S1 with 0.25 units EconoTaq enzyme (Biosearch Technologies, Alexandria, MN, USA), 1× EconoTaq Buffer, 200-µM deoxynucleotide triphosphates, and 0.25-µM primers for all reactions, except *tbx3*^{GR} reactions, which included 2% dimethyl sulfoxide.

Immunostaining

For sections, isolated eyes were fixed in 4% paraformaldehyde/1× PBS for either 30 minutes on ice (for in situ hybridization or green fluorescent protein [GFP] immunostaining) or overnight (for all other immunostaining). The tissue was washed in 1× PBS and then incubated with sucrose (5%, 10%, and 20%). The eyes were then mounted in Tissue-Tek O.C.T. Compound (Sakura Finetek, Torrance, CA, USA) and sectioned (20 µm). We immunostained sections by using conditions that depended on the primary antibody (Supplementary Table S2). Slides were washed three times in 1× PBS and 0.1% Triton X-100 and cover-slipped with FluorSave (MilliporeSigma, Burlington, MA, USA) and 2% 1,4-Diazabicyclo[2.2.2]octane (DABCO; Sigma-Aldrich). Flatmounts were stained with isolectin B4 (IB4) and immunostained with antibodies, as described.[34] Reinforcement labels (5722; Avery Dennison, Mentor, OH, USA) were attached to slides, retinas were placed inside each ring with FluorSave mounting solution and 2% DABCO, and topped with a round coverslip.

RNA In Situ Hybridization

RNA was extracted from mouse retinas using RNAzol RT (Molecular Research Center, Cincinnati, OH, USA), and cDNA was generated using GoScript Reverse Transcriptase (Promega, Madison, WI, USA) according to the manufacturer's protocol. *Tbx3* cDNA was PCR amplified with Herculase II (Fisher Scientific, Waltham, MA, USA) using the following primers: BamH1 mTbx3 forward (5′ aatggatccaCCATGAGCCTCTCCATGAG 3′) and Xho1 mTbx3 reverse (5′ aattctcgagTTAAGGGGACCCGCTG 3′) according to the manufacturer's protocol. The PCR product was cut with BamH1 and Xho1 (New England Biolabs, Ipswich, MA, USA) and cloned directly into pCS2R cut with the same

enzymes. Digoxigenin-labeled sense and antisense cRNA probes were manufactured from linear DNA made using these same two restriction enzymes. In situ hybridization was done as previously described.[35,36]

Microscopy

Images were taken using a Leica DM600B stereomicroscope (Leica, Wetzlar, Germany) outfitted with a MicroPublisher 6 camera (Teledyne Photometrics, Tucson, AZ, USA), and, where applicable, stitched together using Volocity 6.3 software. Confocal images were taken with the Zeiss LSM 780 confocal laser scanning microscope and Zeiss imaging software (Zeiss Group, Oberkochen, Germany). Images of wild-type (WT) and cKO samples were equally processed for brightness and contrast in Photoshop 2022 (Adobe, San Jose, CA, USA). Cell counts and analyses were performed under double-blind conditions. Sample types were revealed when entering numbers into Prism 9.3 (GraphPad, San Diego, CA, USA).

Measurement of Vasculature

We measured the surface area occupied by retinal structures and the volume using Volocity software. The ratio of retinal structure to whole retinal surface was calculated and statistically analyzed. The migration of $Pax2^+$ cells was measured within 500 µm of the dorsal petal (counting 10 cells per sample). The area occupied by $Pax2^+$ cells was measured by adjusting the threshold in ImageJ (National Institutes of Health, Bethesda, MD, USA) and comparing that to the area of the dorsal retina.

Western Immunoblotting

Protein was extracted from both retinas of sibling newborns and processed for western blot analysis as previously described.[37] Anti-TBX3 antibody (1:2000; Bethyl Laboratories, Montgomery, TX, USA) in 5% milk and 0.1% Tween/1× TRIS-buffered saline was used.

Statistical Analysis

Prism 9.3 was used for statistical analysis; legends in the figures indicate the statistical tests used. Measurements were done blind to the genotype of the sample. We normalized data by taking the average WT measurement in each litter and dividing it into each sample in that litter. To determine the density of $OPN4^+$ cells, we divided the retinal petal surface area into the total cells counted (using Volocity software). The average densities for the WT samples were calculated and divided into the density for all sibling samples. To measure the density of $Pax2^+$ cells, we counted an arcuate area of cells within the dorsal and ventral retinal petals. The distal area was determined as 70% of the farthest migrating cell on the petal, the proximal was 60% of the total length, and the sides of the petal marked the edges. Total cells were counted and cells per surface area (mm^2) were calculated (density). Graphs and data are reported as mean ± SEM. Each point on a graph is the average of both eyes from a single animal (*N*).

Results

To determine the expression pattern of *Tbx3* in the embryonic eye, a tamoxifen-inducible Cre was knocked into the *Tbx3* gene locus ($tbx3^{mcm/+}$) and then crossed with the $Rosa^{LacZ}$ reporter line ($tbx3^{mcm/+}$; $Rosa^{LacZ/+}$) (Figs. 1A, 1B).[24] Consistent with earlier studies showing *Tbx3* in mouse neural retina, *LacZ* was expressed at E10.5 and E11.5 in the dorsotemporal region of the optic cup with gradual reduction in the ventral eye.[17,18,38] In situ hybridization to detect *Tbx3* mRNA showed a similar gradient of transcript expression (Figs. 1C, 1D). In newborn mice, we found that *Tbx3* mRNA was confined to the base of the neuroblast layer (Figs. 1E–1E", arrows) and in cells at the inner limiting membrane (Fig. 1E', arrowhead); at P26, we observed that *Tbx3* was evenly distributed throughout the eye, in the innermost cells of the inner limiting membrane (Fig. 1F), in a pattern of expression seen in the human eye at 13 weeks gestation.[18] To better visualize TBX3 expression, we used the recombined $tbx3^{GFP}$ conditional reporter allele $tbx3^{GR/+}$ in which GFP had been knocked into the endogenous *Tbx3* gene (TBX3-GFP).[21] Relatively little GFP staining was detected in WT sibling embryos (Fig. 1G), whereas in $tbx3^{GR/+}$ embryos (Fig. 1H) we detected embryonic TBX3-GFP in the same gradient pattern with a few GFP-positive cells at the optic nerve head (Fig. 1H', arrows). At E13.5, Pax2 was expressed in the optic nerve head in cells fated toward an astroglial lineage.[3,39,40] We detected GFP at low levels co-staining in some $Pax2^+$ cells (Figs. 1H'–H"', arrows; Supplementary Figs. S2A–S2B"), with the Pearson's correlation coefficient for GFP/$Pax2^+$ retinal cells averaging 0.337 ± 0.05 (>4 sections measured per eye; $N = 2$), indicating low correlation. At birth, Pax2 marks astrocyte precursors as they migrate into the retina.[41,42] We flatmounted retinas at P0, immunostained them with anti-Pax2 and GFP antibodies, and then imaged whole retinas (Figs. 1I, 1J; Supplementary Figs. S2C, S2D). Flatmounts of P0 retinas from sibling WT mice had no visible GFP expression, yet TBX3-GFP mice showed GFP/Pax2 colabeling (Figs. 1I, 1J; Supplementary Videos S1, S2). We found no difference in the expression of GFP between dorsal and ventral $Pax2^+$ cells (Figs. 1J', 1J"). Next, we determined the types of cells in which *Tbx3* is expressed by sectioning and staining postnatal $tbx3^{GR/+}$ retinas at P2, P7, and P14 (Figs. 1K, 1L; Supplementary Figs. S2E–S2J').

To determine which postnatal neural cells express *Tbx3*, we continued to use the GFP knock-in. Because Tbx3 was expressed in the ganglion cell layer (Fig. 1E), we first tested for co-expression of GFP with Brn3b and the intrinsically photosensitive ganglion cell marker, Tbr2. All OPN4-expressing intrinsically photosensitive RGCs express Tbr2.[43] At P2, while we failed to see co-expression of Brn3b (Supplementary Fig. S2H), we find GFP co-expressed in about half of $Tbr2^+$ cells (Figs. 1K, 1K', yellow arrows; Supplementary Fig. S2E). To account for the rest of the $Tbx3^+$ cells, we stained retinas with Pax6, which is expressed in amacrine, ganglion cells and Müller glia at postnatal ages.[44,45] We observed that, in the neural retina, GFP was co-expressed with Pax6 at all of these developmental stages (Figs. 1L, 1L'; Supplementary Figs. S2F–S2J'; other data not shown), yet GFP was not co-expressed with the Müller glia marker Sox9 (Supplementary Figs. S2I–S2J'). Together, these data suggest that *Tbx3* is initially expressed in retinal progenitors and possibly some $Pax2^+$ glial progenitors, but later, in the postnatal retina, it is expressed in amacrine and Tbr2-expressing ganglion cells and astrocyte precursors (Figs. 1K', 1L').

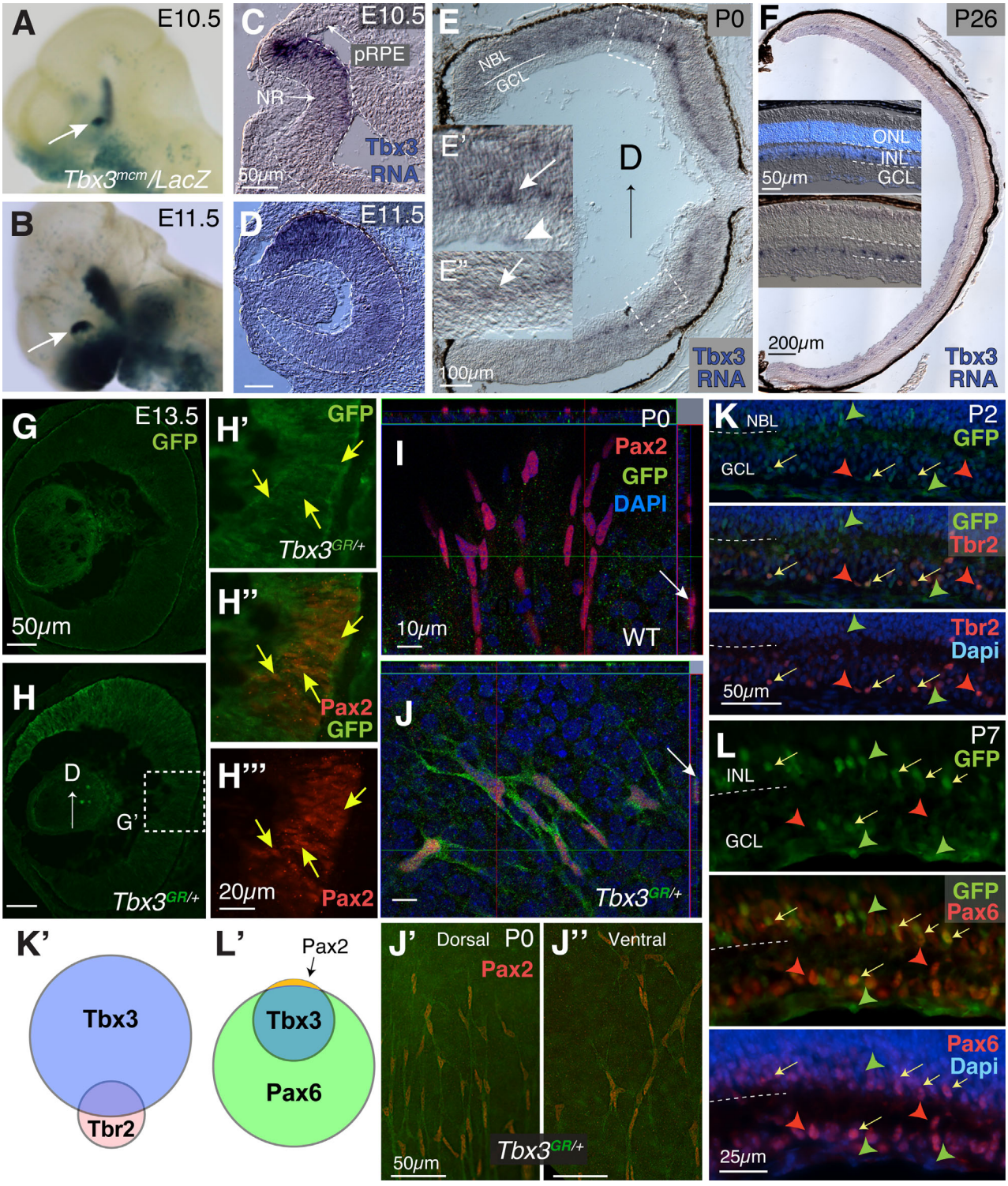

Figure 1. TBX3 expression in the neural retina and efficient conditional knock-out (cKO) using the *BAC-DKK3-Cre* driver. (**A**, **B**) LacZ activity under the control of the endogenous *Tbx3* locus driving Cre recombinase (*tbx3*^{mcm}*/LacZ*). The *arrow* points to the dorsotemporal region of the eye at E10.5 and E11.5 from dams administered tamoxifen by oral gavage when pups reached E8.5. (**C**, **D**) In situ hybridization using *Tbx3* antisense RNA at E10.5 and E11.5. Outline of developing eye; pRPE, presumptive RPE; NR, neural retina. (**E**) *Tbx3* mRNA expression in newborn retina. (**E'**, **E"**) Inlays of dorsal and ventral retinas. *Arrows* point to cells at the base of the neuroblast layer (NBL) and the *arrowhead* to cells at the inner limiting membrane adjacent to the ganglion cell layer (GCL). (**F**) *Tbx3* mRNA expression at P26. *Inlays* show sections with (*above*) and without (*below*) DAPI staining; stained cells occur in the innermost cells of the inner nuclear layer (INL) and in and below the GCL. (**G**, **H**) WT sibling of transgenic embryo expressing GFP under the control of the endogenous *Tbx3* locus (*tbx3*$^{GR/+}$) immunostained with anti-GFP antibody (*green*) at E13.5. *Dashed box* shows the region magnified. (**H'–H'"**) Close-up of boxed region in **G** immunostained with an anti-Pax2 (*red*) and GFP antibodies (see Supplementary Fig. S1 for more images). (**I**) Confocal flatmount image of newborn retina from sibling WT mice (**I**) and *tbx3*$^{GR/+}$ mice (**J**) immunostained with anti-Pax2 and GFP antibodies. Orthogonal view on top and side. In **I**, the *arrow* points to a cell that is positive for Pax2, and in **J** the *arrow* points to a cell that is positive to Pax2 and

GFP. (**J'**, **J"**) Close-up dorsal and ventral images of *Tbx3*$^{GR/+}$ flatmounts stained with Pax2 and GFP. Deconvolved stereomicroscope images. (**K**) Sections of P2 *tbx3*$^{GR/+}$ retinas stained for GFP (*green*) and ipRGC marker Tbr2 (*red*); nuclei stained with DAPI are *blue*. (**K'**) Venn diagram summarizing the quantitated overlap in Tbr2/Tbx3 expression in Supplementary Fig. S1E. (**L**) Sections of P7 retina co-stained with GFP and amacrine/ganglion cell marker Pax6 (*red*) and nuclei (DAPI, *blue*). *Red arrowheads* point to Tbr2 or Pax6; *green arrowheads*, GFP; *yellow arrows*, cells with both. (**L'**) Summary of Tbx3-GFP (*Tbx3*$^{GR/+}$) overlap with Pax6 quantitated in Supplementary Fig. S1F. The *arrow* points to non-retinal cells that are Pax2 positive.

To investigate the effects of *Tbx3* loss on early eye formation, we selected the *BAC-Dkk3-Cre* mouse line.[29] To confirm its specificity, *BAC-Dkk3-Cre* mice were crossed with the Ai9 reporter line that expresses tdTomato in the presence of CRE activity. As previously reported, we found weak expression of the tdTomato reporter in E9.5 optic vesicles (Supplementary Fig. S1A, arrows), which was detected throughout the neural retina and optic stalk and in the lens epithelium by E11.5 (Supplementary Figs. S1C, S1C"). Western blot analysis confirmed the loss of TBX3 protein in the *BAC-Dkk3-Cre;tbx3*$^{\Delta Fl/\Delta Fl}$ retina (Supplementary Figs. S1D, S1E). In *BAC-Dkk3-Cre* postnatal retinas, there was a gap in tdTomato expression in blood vessels, but not the surrounding neurons and astrocytes (arrow, Supplementary Figs. S1F–F"'), confirming that Cre activity was absent in these retinal endothelial cells. To ensure that our protocol detected tdTomato in blood vessels, we used *Tie2-Cre;Ai9* retinal flatmounts stained with the same blood vessel markers, which perfectly matched the expected vascular structures (Supplementary Figs. S1G–S1G"'). Together, these results suggest that *BAC-Dkk3-Cre* drives Cre recombinase in neurons and astrocytes but not endothelial cells. Preliminary observations indicated abnormal blood vessel formation in the eyes of *BAC-Dkk3-Cre;tbx3*$^{\Delta Fl/\Delta Fl}$ mice. Therefore, we investigated the effect of *Tbx3* loss on retinal vasculature development.

Retinal vasculature develops postnatally in mice, and blood vessels reach the edge of the retina by P9.[46,47] Therefore, to determine the effect of *Tbx3* loss on angiogenesis, we stained P9 retinal flatmounts using IB4 to visualize vascular endothelial cells (Figs. 2A, 2A'). *BAC-Dkk3-Cre;tbx3*$^{\Delta Fl/\Delta Fl}$ mice (*Tbx3* cKO) had severe disruption of vasculature development, in that the blood vessels failed to advance to the edges of the retina (Figs. 2B, 2B'). Generally, in WT retinas, the hyaloid vessels (HVs) regress postnatally and are substantially reduced by P8.[11] Although we observed remnants of these vessels in some WT samples (Fig. 2A', arrow), the vessels were easily observed in *Tbx3* cKO retinas (Figs. 2B, 2B'). Measuring retinal surface areas covered by the vasculature (Fig. 2C), we found a decrease in the ventral vascular coverage in comparing *Tbx3* cKO and WT siblings (71% ± 5.9%), yet the dorsal *Tbx3* cKO retina exhibited more loss (24.9% ± 3.0%) (Fig. 2C). These results indicate a requirement for *Tbx3* in the normal development or maintenance of the early postnatal retina vasculature. It is also possible that *Tbx3* loss simply causes a delay in forming the retinal vasculature, so we next looked at blood vessels after they matured.

Retinas were collected from P26 mice to determine the effect of *Tbx3* loss on the mature vascular plexus. In contrast to the WT structure (Figs. 3A–3C), the vascular plexus of *Tbx3* cKO retinas was abnormal (Figs. 3D–3F). Confocal optical sections showed that the superficial layer did not extend to the dorsotemporal peripheral retina in *Tbx3* cKO mice (Figs. 3D, 3F, areas marked by dashed red lines; Supplemental Video S3). In addition, the dorsal vein was thinner and missing from the edge of cKO retinas (compare red arrowheads in Figs. 3G and 3H; see also Supplemental Video S3). The *Tbx3* cKO vascular plexus also appeared less complex when compared to WT siblings (Figs. 3G, 3H). To further define the apparent reduction in complexity, we measured both vasculature branch points and length densities in *Tbx3* cKO and WT animals (Figs. 3I; quantitation shown in Supplementary Fig. S3). We found a reduction in both branch point density (WT, 1537 ± 99 junctions/mm^2; cKO, 1034 ± 106 junctions/mm^2) and vascular length density (WT, 6.48 ± 0.12 mm/mm^2; cKO, 5.20 ± 0.26 mm/mm^2) in mutants (Fig. 3I). Confocal imaging of central retinal sections from controls showed the normal tri-layered vasculature and interplexus branching (Fig. 3J; Supplemental Video S4). In contrast, *Tbx3* cKO retinas lacked the superficial plexus (Fig. 3K; Supplemental Video S5). Cryostat sections show vessels in all three layers in the WT mice (Fig. 3L; Supplementary Fig. S4A), whereas in the absence of *Tbx3* some regions (Fig. 3F, dashed regions) were missing both the superficial and deep layers (Fig. 3M; Supplementary Fig. S4B). Glial fibrillary acidic protein (GFAP) labels Müller glia and astrocytes at this age. We detected less dense GFAP staining in the *Tbx3* cKO retina overall; yet, in the dorsal tip, we found a slight elevation of GFAP tendrils in the retina, along with a thinner outer nuclear layer in the mutants (Fig. 3M, bracket). This staining is consistent with activated Müller glia responding to the thinning retina. Less GFAP staining suggests fewer astrocytes in the dorsal *Tbx3* cKO retina. Together, these results indicate that the formation of a normal adult retinal vasculature requires *Tbx3*.

If the reduction in angiogenesis in the *Tbx3* cKO begins at this early time point, then we would expect the lattice to be disrupted in mutant mice. Flatmounts at P2 showed reduced endothelial cells and astrocytes in the *Tbx3* cKO retina (Figs. 4B, 4B'). Retinal astrocyte precursors express the paired-box transcription factor Pax2 and receptor platelet-derived growth factor alpha (PDGFRα), but, as they mature they do not express GFAP.[41,42] We found stunted migration and fewer Pax2$^+$ astrocyte precursors in the dorsal retinas at P2 (Fig. 4C–4F). We observed a 33% reduction in Pax2$^+$ cell density in dorsal retinas (control 696 ± 50 cells vs. cKO 462 ± 49 cells) and a corresponding increase of 38% in the ventral retinas (control 624 ± 76 cells vs. cKO 861 ± 72 cells). We further reasoned that lattice formation may recover if TBX3 is only required at this initial stage and therefore next looked at older animals.

By P9, astrocytes reached the edge of the WT retina (Fig. 5A) yet failed to do so in the cKO (Fig. 5B). Even at 1 month of age, astrocytes failed to reach the dorsal edge of the cKO retinas (compare Fig. 5C to Figs. 5D and 5D'). By double labeling astrocytes and endothelial cells, we found an abnormal vascular plexus in areas without a stereotypical astrocyte lattice (Figs. 5D'–5D"'). We compared the surface area occupied by astrocytes at P9 and P30, normalized to the average WT retinal surface area. We observed a statistically significant difference between WT and *Tbx3* cKO retinas at P9 and P30 (P9 WT, 1.0 ± 0.01; P9 cKO, 0.58 ± 0.02; P30

Investigative Ophthalmology & Visual Science

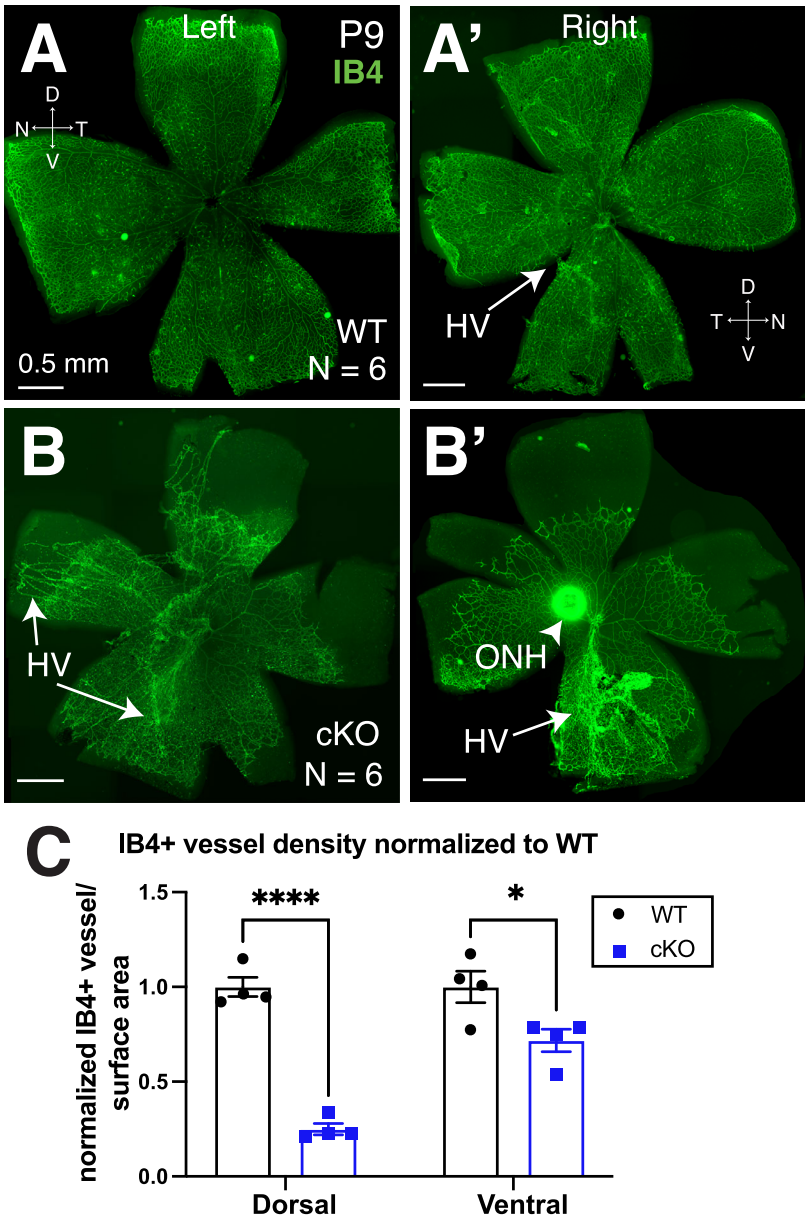

Figure 2. *Tbx3* loss results in abnormal blood vessel development. Flatmount P9 retinas from WT mice (**A**, **A'**) and conditional *Tbx3* knockout retinas (cKO) (**B**, **B'**) stained with isolectin GS-B4 (IB4, *green*) in left and right eyes. *Arrows* indicate the locations of hyaloid vessels (HVs). (**C**) Ratio of the vascularized to total retinal surface area in the dorsal and ventral retina normalized to average WT in each litter. A two-way ANOVA with Šidák's multiple comparisons test was used. $^{*}P = 0.01$; $^{****}P \leq 0.0001$.

WT, 0.97 ± 0.01; P30 cKO, 0.76 ± 0.03) (Fig. 5E). Nevertheless, we also observed significant growth between P9 and P30 ($P < 0.001$) in the cKO retinas, indicating that signals promoting vascular formation persist in the absence of TBX3 (Fig. 5E). These results indicate that astrocytes require TBX3 to form the astrocytic lattice required for normal retinal vasculature formation. Astrocyte lattice formation can also be disrupted with the loss of RGCs, as in the *Atoh7* knockout retina. These mice grow a severely stunted astrocytic lattice.[4,48] Thus, it is possible that TBX3 is indirectly affecting astrocytes by functioning within ganglion cells. Previous studies have also shown that hyaloid vessel regression is dependent on signals from intrinsically photosensitive RGCs.[10,11] We observed that hyaloid vessels persisted in the mutant retina (Figs. 2B, 2B'; Fig. 5B). Therefore, we next investigated whether RGC formation requires TBX3.

We found that optic nerves were significantly thinner in cKO mice compared to their WT littermates (Fig. 6A–6C), measuring 71% ± 3.9% of the average WT optic nerve (Fig. 6D). Using the anti-Islet1/2 antibody, we observed a significant decrease in dorsal Islet1/2-positive RGCs in the cKO retina, but no difference in the ventral region (dorsal WT, 37.7 ± 2.8 cells; dorsal cKO, 27.7 ± 2.4 cells) (Figs. 6E–6G). This suggests that *Tbx3* is required by a subset of Islet1/2-expressing dorsal RGCs. Islet1 is thought to regulate the formation of most RGCs, including melanopsin-expressing (OPN4) ipRGCs.[43] As we had identified co-staining of Tbx3-GFP and Tbr2, we wondered if $Tbr2^{+}$ RGCs were affected by *Tbx3* loss in the newborn retina. We found a significant decrease in these cells (ratio of cells/average WT: WT, 1.00 ± 0.06; cKO, 0.68 ± 0.09) (Figs. 7A–7C). To determine if loss

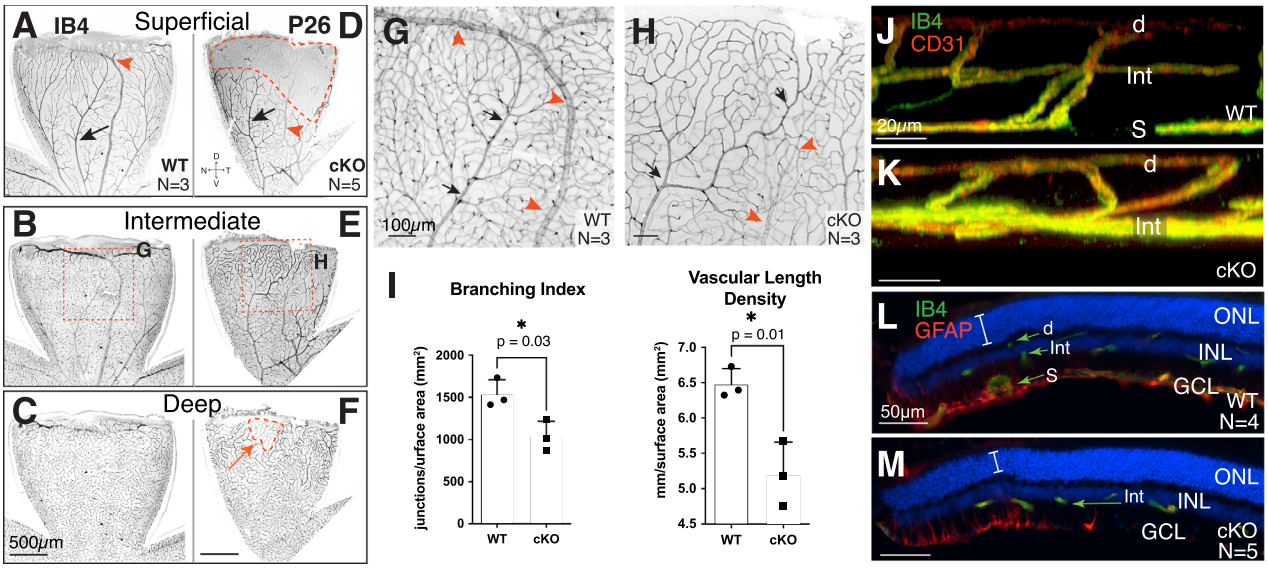

Figure 3. *Tbx3* cKO retina failed to form superficial plexus in the adult dorsal retina. (**A**–**F**) Confocal flatmount images of P26 dorsal retinas from WT (**A**–**C**) and cKO (**D**–**F**) mice stained with isolectin GS-B4 (IB4). Confocal images are inverted. The superficial (**A**, **D**), intermediate (**B**, **E**), and deep (**C**, **F**) plexus from the same retinal flatmounts are shown. (**G**, **H**) Maximal projection images from a stereomicroscope simultaneously showing all three plexi from the region indicated in **B** and **E**. Arteries (*black arrows*) and veins (*red arrowheads*) in each panel are marked. (**I**) Branching index (branch points/retinal surface area) and vascular length density (vessel length/retinal surface area) from maximum projections images (see Supplementary Fig. S2 for quantitation). Statistical significance was determined using an unpaired, two-tailed *t*-test; *P* values are shown on the graph. (**J**, **K**) Still, three-dimensional, rendered confocal images of retinal plexus in dorsal retina of WT (**J**) and cKO (**K**) mice stained with IB4 (*green*) and anti-CD31 antibody (*red*). (**L**, **M**) Transverse cryostat sections of P26 retina stained with IB4 (*green*) and anti-GFAP antibody (*red*) to mark endothelial cells and astrocytes, respectively. The superficial vascular plexus (S), intermediate vascular plexus (Int), and deep vascular plexus (d) are marked; the outer nuclear layer (ONL), inner nuclear layer (INL), and GCL can be seen with the nuclei marker DAPI (*blue*). Note that the anti-GFAP (raised in mouse) antibody lightly stained the vascular cells, as these mice were not perfused.

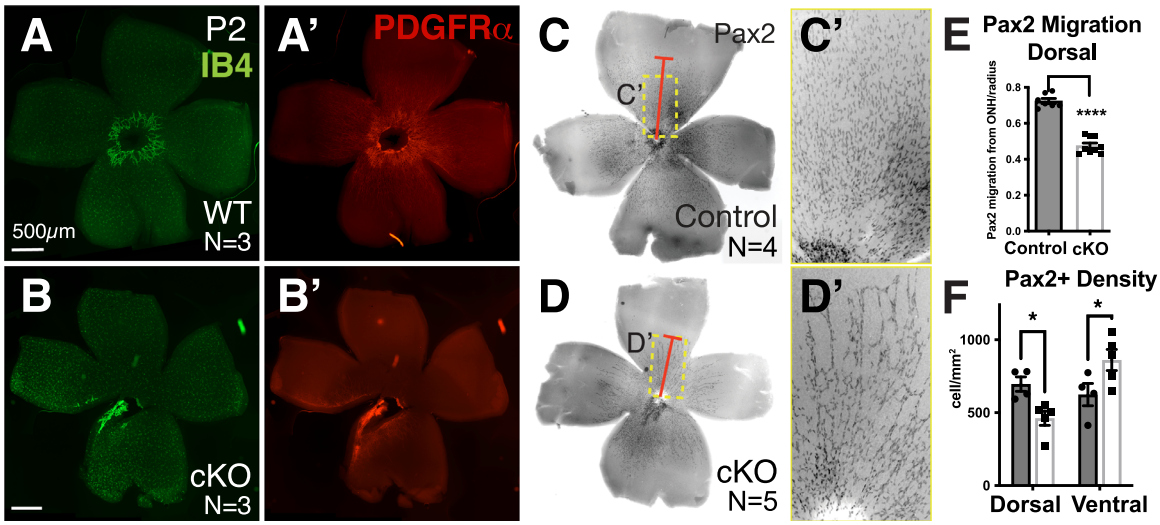

Figure 4. Fewer astrocyte precursors were observed in *Tbx3* cKO retinas, starting as early as P2. (**A**, **B**) Endothelial cells are marked with IB4 (*green*) in WT and *Tbx3* cKO flatmounted retinas at P2. (**A'**, **B'**) Same samples immunostained for astrocyte precursors using anti-PDGFR*α* antibody. (**C**, **D**) Inverse images of flatmount retinas from P2 WT and *Tbx3* cKO mice stained with a second astrocyte precursor marker, anti-Pax2 antibody (*black*). The *red bar* marks $Pax2^+$ cells farthest away from the optic nerve head in each panel. The *dashed yellow box* indicates images magnified in panels **C'** and **D'**. (**E**) Quantitation of $Pax2^+$ cells farthest away from the optic nerve head in heterozygote (*gray* indicates control, $N = 4$) and cKO (*white bar*, $N = 5$) retinas. Distance is an averaged measure of 10 cells per dorsal and another 10 per ventral. (**F**) Graph shows quantitation of the percentage of surface area occupied by dorsal and ventral retinas in control (*gray*) and cKO (*white*) retinas. (**G**) Quantitation of $Pax2^+$ cell density in dorsal and ventral regions of control (*gray*) and cKO (*white*) retinas. Statistical significance was determined using an unpaired *t*-test (**E**) and a two-way ANOVA with Šídák's multiple comparisons test (**F**). *$P > 0.05$; **** $P < 0.0001$.

Investigative Ophthalmology & Visual Science

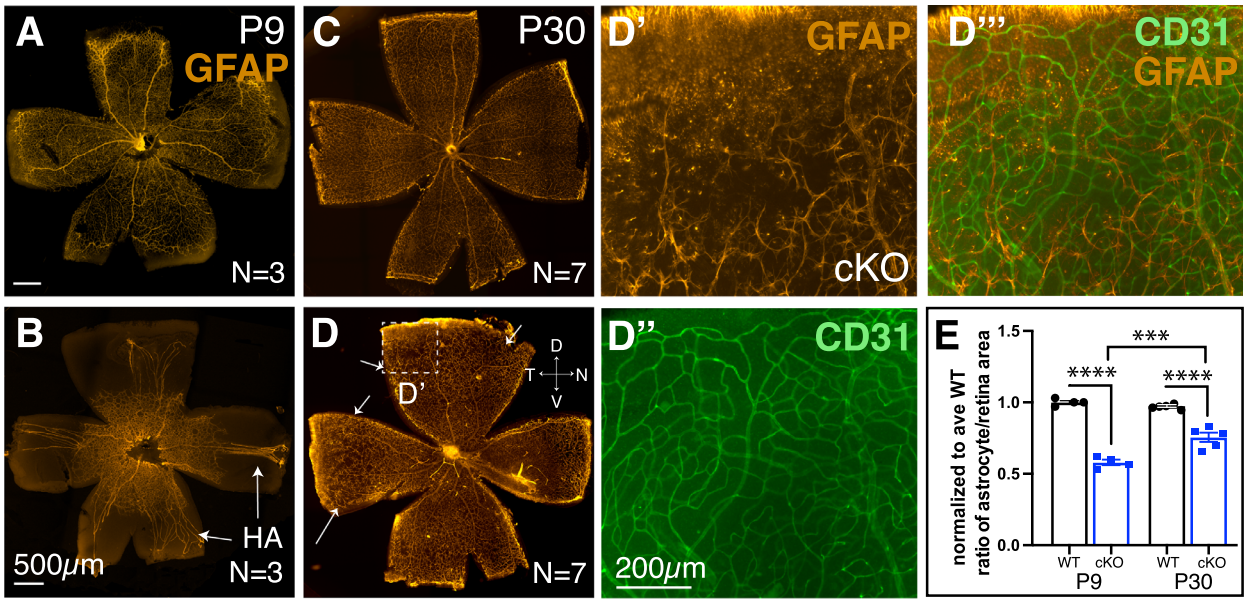

Figure 5. Astrocyte lattice failed to form in the dorsal–temporal *Tbx3* cKO retina. (**A**, **B**) Flatmount P9 retinas immunostained with mature astrocyte marker, anti-GFAP antibody. *Arrows* point to the hyaloid artery (HA). (**C**, **D**) Flatmount P30 retinas from WT and cKO mice; in **D**, the *arrows* indicate lattice thinning. (**D'**–**D'''**) Magnified view of boxed region in **D** showing a dorsal region where the astrocyte lattice failed to reach the retinal edge. (**D'**) Astrocytes, GFAP (*orange*); (**D''**) endothelial cells, IB4 (*green*); and (**D'''**) overlay. (**E**) Graph quantifying the normalized ratio of astrocyte occupation compared to the retinal surface area for WT and cKO retinas. Dorsal is *up* in all panels. Statistical significance was determined using ordinary two-way ANOVA with Tukey multiple comparisons. ***$P \leq 0.001$; ****$P \leq 0.000.1$.

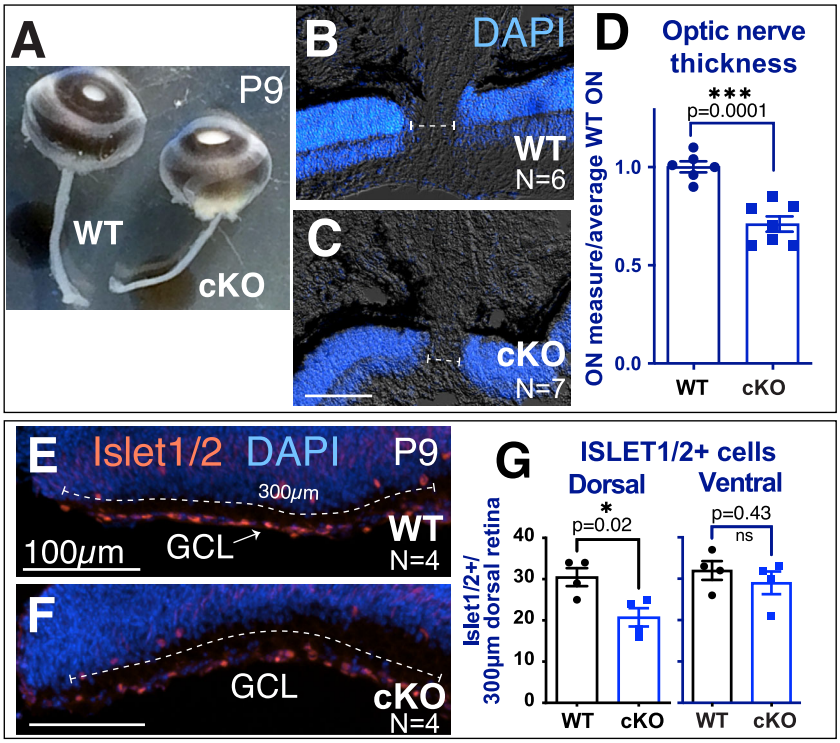

Figure 6. Dorsal-specific loss of RGCs with loss of *Tbx3*. (**A**) Snapshot of whole eyes with optic nerves from P9 WT and cKO siblings. (**B**, **C**) Sections of WT and cKO eyes stained with nuclei marker (DAPI) to visualize neural retina. The *dashed line* indicates optic nerve thickness in each sample. (**D**) Graph quantitating the optic nerve thickness in WT and cKO eyes. (**E**, **F**) Transverse cryostat sections of P9 WT and cKO dorsal tip immunostained with anti-Islet1/2 antibody. The numbers of Islet1/2-positive cells in the first 300 μm of the most dorsal and ventral retina were counted (*dashed line*). (**G**) Graphs of the Islet1/2-positive cells in the dorsal and ventral regions. Statistical significance was measured using an unpaired, two-tailed *t*-test for the graphs in **D** and **G**.

Investigative Ophthalmology & Visual Science

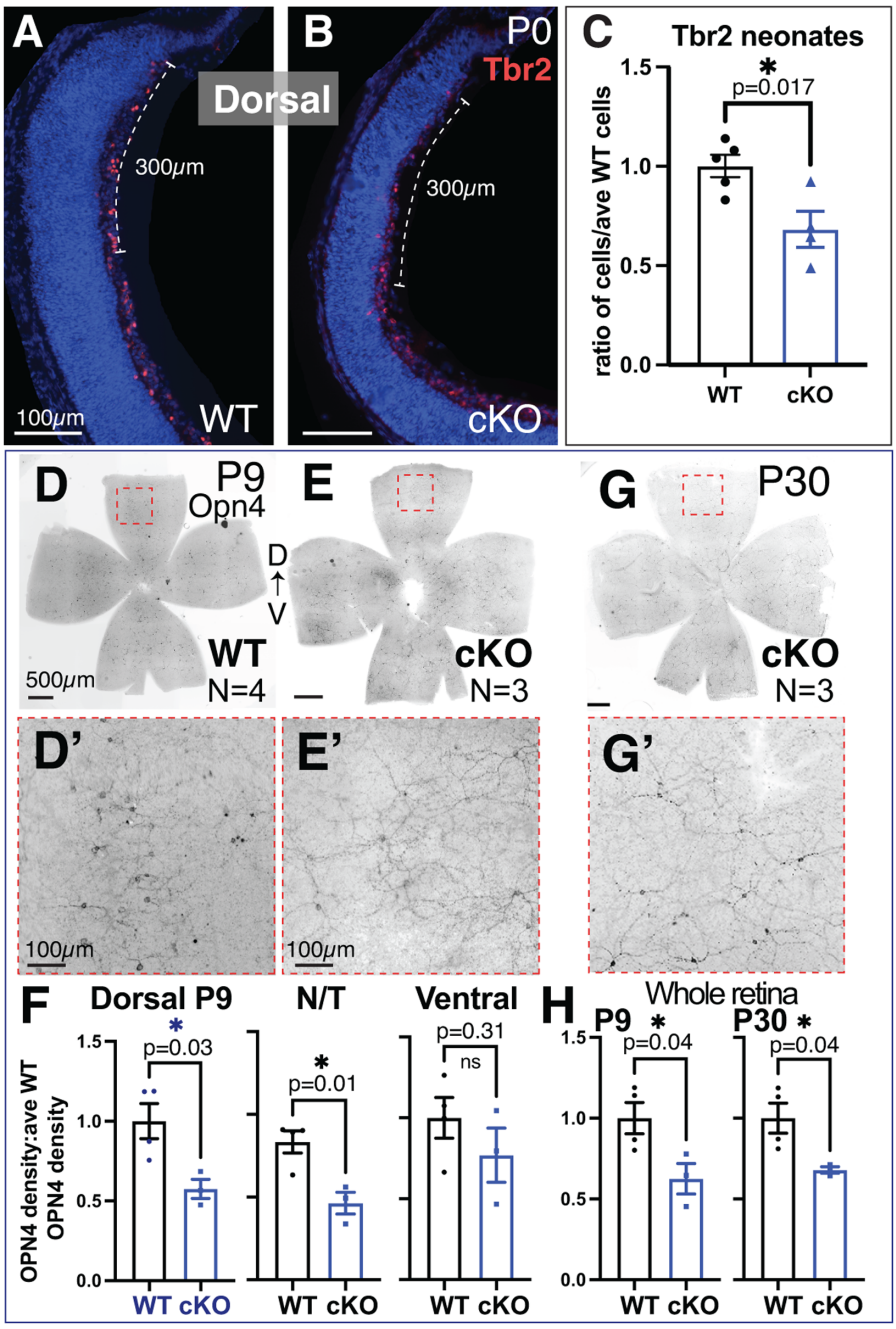

Figure 7. Reduction of ipRGCs in dorsal *Tbx3* cKO retinas starting at birth. (**A**, **B**) Cryostat sections (20 µm) of P0 retinas from WT and *Tbx3* cKO mice immunostained with an anti-Tbr2 antibody marking early ipRGCs. *Dashed bar* indicates 300-µm area of Tbr2$^+$ cells counted in the dorsal and central retinal sections. (**C**) Graph of the quantitation of Tbr2$^+$ cells in P0 and P1 dorsal retinas (WT, $N = 5$; cKO, $N = 4$). An unpaired, two-tailed *t*-test was used to determine statistical significance. (**D–E'**) Inverse images of P9 flatmount WT and cKO retinas immunostained with anti-OPN4 antibody marking differentiated ipRGCs. The *dashed box* shows the area magnified in **D'** and **E'**. Density of cells was measured in dorsal, nasal/temporal (N/T), and ventral petals and normalized to WT siblings. (**F**) Graphs showing quantitation of OPN4$^+$ cells in each region. (**G**) Inverse image of P30 cKO flatmount with magnified area (*dashed box*) shown in panel **G'**. (**H**) Graphs of OPN4$^+$ cells per whole retina of P9 (WT, $N = 4$; cKO, $N = 3$) and P30 samples (WT, $N = 4$; cKO, $N = 3$). Unpaired, two-tailed *t*-tests were used to determine statistical significance; *P* values are shown on the graphs in **C**, **F**, and **H**.

of these cells persisted, we stained flatmounts with the anti-OPN4 antibody and measured the density of OPN4$^+$ cells for each sample, normalized to the average WT control. When blood vessels were stunted at P9, we observed significant reduction of ipRGC density in the dorsal petals (WT, 1.00 ± 0.11; cKO, 0.57 ± 0.06) and nasal/temporal petals (WT, 0.83 ± 0.07; cKO, 0.46 ± 0.06), but not in the ventral petals (Figs. 7D–7F). Overall, we found significantly fewer ipRGCs in cKO retinas at P9 (WT, 1.00 ± 0.10; cKO, 0.63 ± 0.09). This difference persisted when measured at P30 (WT, 1.00 ± 0.09; cKO, 0.68 ± 0.02), suggesting that the reduction in ipRGCs was not due to a delay of differentiation

(Figs. 7G–7H). Together, these results indicate that TBX3 is required for a subset of OPN4-expressing ipRGCs in the dorsal half of the retina, which control vascular formation in this region.

Discussion

To the best of our knowledge, our results provide the first evidence that TBX3 is required for mammalian eye formation. We have found that *Tbx3* mRNA and protein are expressed in embryonic retinal progenitors and postnatally in retinal amacrine cells, Tbr2-expressing ganglion cells, and astrocyte precursors. When we removed *Tbx3* from the embryonic optic cup, the hyaloid vessels persisted in P9 mice and retinal vascular formation was stunted. At P9, the vascular defect was found throughout the retina but was more severe in the dorsal region. The dorsal vascular plexus continued to be affected by *Tbx3* loss in the older animals, including losses of the superficial layer of the vascular plexus and the astrocyte lattice. We observed that, in the absence of *Tbx3*, fewer astrocyte precursors were present in the dorsal retina. As the retina matured, astrocyte lattice formation recovered in all but the dorsal region. To our knowledge, this is the first report of localization of the defect to the dorsal intraretinal vasculature. In contrast, loss of Aldh1a1, also expressed in dorsal retinal neurons, affects the dorsal choroidal or outer retinal vasculature.[49] In the dorsal neural retina of *Tbx3* conditional mutants, we found fewer Tbr2-expressing RGCs at birth, when astrocytes were beginning to enter the retina. One current hypothesis is that these neurons fail to attract or stimulate the proliferation and/or migration of astrocyte precursors that form the dorsal lattice. Evidence in support of this hypothesis is the reduction in astrocyte density that we observed in the dorsal retina at P2. In contrast, our data could also suggest that TBX3 may function within astrocytes, controlling their development and/or migration, and the loss of *Tbx3* in retinal progenitor cells, which affects dorsal RGCs, simply causes hyaloid vessel persistence at P9 in the *Tbx3* cKO retina. The fact that we observed abnormal vascular plexus and decreased astrocyte density in the dorsal retina supports the hypothesis that the underlying defect is the loss of dorsal RGCs. In future studies, we will remove *Tbx3* from only the neural retina or developing astrocytes and measure each effect on retinal vascular formation.

Patients with syndromes such as Norrie disease or FEVR develop hypovascular retinas that lead to congenital blindness.[50] These diseases have been associated with mutations in Wnt/Norrie signaling pathway ligands (*LRP5* and *NDP*), a receptor (FZ4), and a co-receptor (*TSPAN12*), as well as a kinesin family member 11 (*KIF11*).[6–9] Mutations found in these proteins have been studied using mouse models of these mutant alleles.[50–55] Canonical Wnt signaling occurs when Wnt ligands bind to their receptors, which leads to stabilizing β-catenin that can regulate target downstream genes. Although most of these factors work in the canonical Wnt/Norrie signaling pathway, *KIF11* has been shown to function independently from β-catenin signaling in retinal angiogenesis.[50] In separate studies, TBX3 has been shown to work in Wnt signaling and with a kinesin protein. In pull-down assays, TBX3 has direct interaction with another kinesin family member, KIF7, and affects its function.[24] In vivo, TBX3 has been shown to work with, or downstream of, the Wnt signaling pathway in ureter, lung, and human colorectal cancer.[23,26,56] In future studies, we plan to determine in which molecular pathway TBX3 functions.

In addition to hypovascularization, patients with FEVR can also have persistent hyaloid vessels.[57–61] In mice, persistent hyaloid vessels has also been found with the loss of melanopsin (*OPN4*); however, in these mutant mice, hyaloid vessels are eventually absorbed, and the retina is hypervascular rather than hypovascular.[11] In contrast, the *Tbx3* cKO, which has loss of OPN4$^+$ cells, has persistent hyaloid vessels, as well as a hypovascular retina; therefore, the *Tbx3* cKO vascular defect is due to more than a loss of OPN4$^+$ cells. Along with FEVR, these phenotypes are also present in a mouse model of ROP, in which neonatal pups are exposed to elevated oxygen levels from P0 to P4.[62] In these mouse models of ROP, angiogenesis is globally affected, such that in one study only about 25% of the entire retinal surface was covered by P8.[62] In comparison, vessels covered approximately 25% of the dorsal *Tbx3* cKO retina. Therefore, it is possible that TBX3 is required for the hypoxia signaling pathway either in neurons or in astrocytes. Moreover, this regional change is intriguing, as the blood vessels of infants with ROP reach the nasal ora serrata but leave a gap in the temporal edge, called Zone III.[63] The current thinking is that the avascular area is linked to gestational age because there is an abrupt stop of angiogenesis at birth.[64] It is also possible that regional control of vascular growth occurs, which may be understood by knowing the molecular pathways controlled by regionally expressed factors, such as TBX3. The similarities between the phenotypic changes we observed in the conditional *Tbx3* knockout mouse and those in patients with FEVR or ROP suggest the exciting possibility that the *Tbx3* cKO may serve as a new mouse model for hypovascular diseases.

It is important to note that the phenotype of the *Tbx3* cKO also deviates somewhat from these human diseases and previous mouse models of hypovascularization. In FEVR patients, vascular changes can vary from minimal changes to the peripheral retina to becoming exudative and lead to retinal detachments.[65] In the *Tbx3* cKO adult, we failed to observe leaky vessels when we injected tail veins with fluoresceine and imaged their blood vessels (data not shown). This suggests that *Tbx3* may be required in the neural retina and astrocytes for forming the stereotypic tri-layered vascular structure but not blood–retinal barrier formation. Furthermore, oxygen-induced retinopathy models of ROP show neovascularization, which we did not observe. Finally, we find that the superficial vascular plexus failed to form in the dorsal peripheral retina, whereas the intermediate and deep layers remained intact, a finding that again deviates from current mouse models of hypovascular disease.[66,67] It is because of these differences that the *Tbx3* cKO is an interesting model to study further. In the future, we hope to uncover the underlying molecular mechanism that drives the malformed vascular plexus.

We discovered that TBX3-GFP is expressed in astrocyte precursors. We found that *Tbx3* loss causes a reduction in astrocyte precursors in the newborn retina. Astrocytes arise from the optic disc progenitor zone that surrounds the optic nerve disc.[42,68] During migration into the retina, they proliferate prior to contact with endothelial cells; thereafter, the endothelial cells cause their differentiation and they cease proliferation.[68] Our results could be explained by either a reduction in astrocyte precursor proliferation or reduced migration due to corrupt cues from the neural retina lacking *Tbx3*. RGCs release platelet-derived growth factor A-chain (PDGF-A), which attracts astrocytes, but PDGF-A also causes proliferation of these cells.[69] As we have also observed a loss of RGCs in the dorsal retina, it is possible that the loss of

Tbx3 indirectly affects astrocyte proliferation/migration. It is also possible that in astrocyte precursors TBX3 contributes to the regulation of a gene that controls astrocyte proliferation, such as the transcription factor Tailless (*Tlx*).[70,71] We previously found that misexpression of frog *Tbx3* (also known as ET for "Eye T-box") induced *Tll* expression.[15] It will be important to investigate the role of TBX3 in regulating *Tlx* expression and astrocyte proliferation and/or migration.

Later, in the differentiated retina, we found truncation of the astrocytic lattice in the dorsal–temporal region. Blood vessels were growing into the area, but they failed to form a superficial plexus. Endothelial cells build the superficial plexus in response to the chemical and structural cues of the underlying astrocytes.[72–77] Therefore, it is logical that the loss of dorsal astrocytes due to loss of *Tbx3* would lead to superficial plexus loss in that region. Finding dorsal intermediate blood vessels in the absence of the superficial and sometimes deep layers is curious. The deep plexus formation has been linked to spontaneous activity from cholinergic starburst amacrine cells.[78] Meanwhile, the formation of the superficial and deep, but not intermediate, plexus requires the activity of the hypoxic response pathway (via the von Hippel–Lindau factor found in amacrine and horizontal cells).[79] A recent study used single-cell PCR to generate a genetic regulatory network in the mouse retina; in the E18 to P2 tissue, *Tbx3* was found to be expressed by amacrine and Müller glia cells.[80] In the current study, we found TBX3 in amacrine and ganglion cells but not in Müller glia (Supplemental Fig. S1E). It may be that TBX3 is expressed in Müller glial precursors, as we examined overlapping expression of Tbx3-GFP with Sox9 at P14, well after the single-cell analysis had been performed.[80] Further lineage tracing using the Tbx3-GFP mice at earlier ages, with new Müller glial precursor markers, could resolve this discrepancy. Overexpression of TBX3 in retinal progenitors at P0 led to an increase of amacrine cells, retinal ganglion cells, Müller glia, and bipolar cells but repressed formation of rod photoreceptors.[80] Therefore, in future studies, we will determine the effect of *Tbx3* loss on all types of retinal neurons.

Acknowledgments

The authors thank Jason Shandler, Robertha Barnes, Amanda Bielecki, Abigail Snow, Stephen Sanabria, and Dominica Colavito for their excellent technical assistance. We also thank Arvydas Matiukas, PhD, for his assistance in using the confocal microscope in the Neuroscience Microscopy Core. The anti-Islet1/2 and anti-Pax6 antibodies were obtained from the Developmental Studies Hybridoma Bank, created by the National Institute of Child Health and Human Development of the National Institutes of Health and maintained at The University of Iowa, Department of Biology (Iowa City, IA, USA).

Supported by grants from the National Institutes of Health (R21 EY029114 to ASV; R01 EY012676 to WJB; R21 EY030654 to MEZ; R01 EY024373 to SF) and by grants to the Ophthalmology and Visual Sciences Department from Research to Prevent Blindness (unrestricted award) and the District 20-Y Lions Club.

Disclosure: **M.L. Derbyshire**, None; **S. Akula**, None; **A. Wong,** None; **K. Rawlins**, None; **E.B. Voura**, None; **W.J. Brunken**, None; **M.E. Zuber**, None; **S. Fuhrmann**, None; **A.M. Moon**, None; **A.S. Viczian**, None

References

1. Selvam S, Kumar T, Fruttiger M. Retinal vasculature development in health and disease. *Prog Retin Eye Res*. 2018;63:1–19.
2. Sun Y, Smith LEH. Retinal vasculature in development and diseases. *Annu Rev Vis Sci*. 2018;4:101–122.
3. Tao C, Zhang X. Development of astrocytes in the vertebrate eye. *Dev Dyn*. 2014;243(12):1501–1510.
4. O'Sullivan ML, Puñal VM, Kerstein PC, et al. Astrocytes follow ganglion cell axons to establish an angiogenic template during retinal development. *Glia*. 2017;65(10):1697–1716.
5. Paisley CE, Kay JN. Seeing stars: Development and function of retinal astrocytes. *Dev Biol*. 2021;478:144–154.
6. Li JK, Li Y, Zhang X, et al. Spectrum of variants in 389 Chinese probands with familial exudative vitreoretinopathy. *Invest Ophthalmol Vis Sci*. 2018;59(13):5368–5381.
7. Rao FQ, Cai XB, Cheng FF, et al. Mutations in *LRP5*, *FZD4*, *TSPAN12*, *NDP*, *ZNF408*, or *KIF11* genes account for 38.7% of Chinese patients with familial exudative vitreoretinopathy. *Invest Ophthalmol Vis Sci*. 2017;58(5):2623–2629.
8. Tang M, Sun L, Hu A, et al. Mutation spectrum of the *LRP5*, *NDP*, and *TSPAN12* genes in Chinese patients with familial exudative vitreoretinopathy. *Invest Ophthalmol Vis Sci*. 2017;58(13):5949–5957.
9. Tauqeer Z, Yonekawa Y. Familial exudative vitreoretinopathy: Pathophysiology, diagnosis, and management. *Asia Pac J Ophthalmol (Phila)*. 2018;7(3):176–182.
10. Nguyen MT, Vemaraju S, Nayak G, et al. An opsin 5-dopamine pathway mediates light-dependent vascular development in the eye. *Nat Cell Biol*. 2019;21(4):420–429.
11. Rao S, Chun C, Fan J, et al. A direct and melanopsin-dependent fetal light response regulates mouse eye development. *Nature*. 2013;494(7436):243–246.
12. Motahari Z, Martinez-De Luna RI, Viczian AS, Zuber ME. Tbx3 represses bmp4 expression and with Pax6 is required and sufficient for retina formation. *Development*. 2016;143(19):3560–3572.
13. Weidgang CE, Russell R, Tata PR, et al. TBX3 directs cell-fate decision toward mesendoderm. *Stem Cell Reports*. 2013;1(3):248–265.
14. Wong K, Peng Y, Kung HF, He ML. Retina dorsal/ventral patterning by *Xenopus* TBX3. *Biochem Biophys Res Commun*. 2002;290(2):737–742.
15. Zuber ME, Gestri G, Viczian AS, Barsacchi G, Harris WA. Specification of the vertebrate eye by a network of eye field transcription factors. *Development*. 2003;130(21):5155–5167.
16. Takabatake Y, Takabatake T, Takeshima K. Conserved and divergent expression of *T-box* genes *tbx2-tbx5* in *Xenopus*. *Mech Dev*. 2000;91(1-2):433–437.
17. Chapman DL, Garvey N, Hancock S, et al. Expression of the T-box family genes, *tbx1-tbx5*, during early mouse development. *Dev Dyn*. 1996;206(4):379–390.
18. Sowden JC, Holt JK, Meins M, Smith HK, Bhattacharya SS. Expression of *Drosophila omb*-related T-box genes in the developing human and mouse neural retina. *Invest Ophthalmol Vis Sci*. 2001;42(13):3095–3102.
19. Davenport TG, Jerome-Majewska LA, Papaioannou VE. Mammary gland, limb and yolk sac defects in mice lacking *Tbx3*, the gene mutated in human ulnar mammary syndrome. *Development*. 2003;130(10):2263–2273.
20. Frank DU, Emechebe U, Thomas KR, Moon AM. Mouse TBX3 mutants suggest novel molecular mechanisms for Ulnar-mammary syndrome. *PLoS One*. 2013;8(7):e67841.
21. Frank DU, Carter KL, Thomas KR, et al. Lethal arrhythmias in Tbx3-deficient mice reveal extreme dosage sensitivity of

cardiac conduction system function and homeostasis. *Proc Natl Acad Sci U S A*. 2012;109(3):154–163.
22. Barry DM, McMillan EA, Kunar B, et al. Molecular determinants of nephron vascular specialization in the kidney. *Nat Commun*. 2019;10(1):5705.
23. Aydoğdu N, Rudat C, Trowe MO, et al. TBX2 and TBX3 act downstream of canonical WNT signaling in patterning and differentiation of the mouse ureteric mesenchyme. *Development*. 2018;145(23):dev171827.
24. Emechebe U, Kumar PP, Rozenberg JM, et al. T-box3 is a ciliary protein and regulates stability of the Gli3 transcription factor to control digit number. *eLife*. 2016;5:e07897.
25. Kumar PP, Franklin S, Emechebe U, et al. TBX3 regulates splicing in vivo: A novel molecular mechanism for Ulnar-mammary syndrome. *PLoS Genet*. 2014;10(3):e1004247.
26. Lüdtke TH, Rudat C, Wojahn I, et al. Tbx2 and Tbx3 act downstream of Shh to maintain canonical Wnt signaling during branching morphogenesis of the murine lung. *Dev Cell*. 2016;39(2):239–253.
27. Quarta C, Fisette A, Xu Y, et al. Functional identity of hypothalamic melanocortin neurons depends on Tbx3. *Nat Metab*. 2019;1(2):222–235.
28. Kaiser M, Wojahn I, Rudat C, et al. Regulation of otocyst patterning by *tbx2* and *Tbx3* is required for inner ear morphogenesis in the mouse. *Development*. 2021;148(8):dev.195651.
29. Sato S, Inoue T, Terada K, et al. Dkk3-Cre BAC transgenic mouse line: A tool for highly efficient gene deletion in retinal progenitor cells. *Genesis*. 2007;45(8):502–507.
30. Vigouroux RJ, Cesar Q, Chédotal A, Nguyen-Ba-Charvet KT. Revisiting the role of Dcc in visual system development with a novel eye clearing method. *eLife*. 2020;9:e51275.
31. Biswas S, Watters J, Bachay G, et al. Laminin-dystroglycan signaling regulates retinal arteriogenesis. *FASEB J*. 2018;32(11):fj201800232R.
32. Kisanuki YY, Hammer RE, Miyazaki J, Williams SC, Richardson JA, Yanagisawa M. Tie2-Cre transgenic mice: A new model for endothelial cell-lineage analysis in vivo. *Dev Biol*. 2001;230(2):230–242.
33. Park EJ, Sun X, Nichol P, Saijoh Y, Martin JF, Moon AM. System for tamoxifen-inducible expression of cre-recombinase from the *Foxa2* locus in mice. *Dev Dyn*. 2008;237(2):447–453.
34. Gnanaguru G, Bachay G, Biswas S, Pinzon-Duarte G, Hunter DD, Brunken WJ. Laminins containing the $\beta 2$ and $\gamma 3$ chains regulate astrocyte migration and angiogenesis in the retina. *Development*. 2013;140(9):2050–2060.
35. Viczian AS, Vignali R, Zuber ME, Barsacchi G, Harris WA. *XOtx5b* and *XOtx2* regulate photoreceptor and bipolar fates in the *Xenopus* retina. *Development*. 2003;130(7):1281–1294.
36. Martinez-De Luna RI, Ku RY, Lyou Y, Zuber ME. Maturin is a novel protein required for differentiation during primary neurogenesis. *Dev Biol*. 2013;384(1):26–40.
37. Wong KA, Trembley M, Abd Wahab S, Viczian AS. Efficient retina formation requires suppression of both Activin and BMP signaling pathways in pluripotent cells. *Biol Open*. 2015;4(4):573–583.
38. Behesti H, Holt JK, Sowden JC. The level of BMP4 signaling is critical for the regulation of distinct T-box gene expression domains and growth along the dorso-ventral axis of the optic cup. *BMC Dev Biol*. 2006;6:62.
39. Bosze B, Suarez-Navarro J, Soofi A, Lauderdale JD, Dressler GR, Brown NL. Multiple roles for *Pax2* in the embryonic mouse eye. *Dev Biol*. 2021;472:18–29.
40. Soukkarieh C, Agius E, Soula C, Cochard P. Pax2 regulates neuronal–glial cell fate choice in the embryonic optic nerve. *Dev Biol*. 2007;303(2):800–813.
41. Chu Y, Hughes S, Chan-Ling T. Differentiation and migration of astrocyte precursor cells and astrocytes in human fetal retina: Relevance to optic nerve coloboma. *FASEB J*. 2001;15(11):2013–2015.
42. Mi H, Barres BA. Purification and characterization of astrocyte precursor cells in the developing rat optic nerve. *J Neurosci*. 1999;19(3):1049–1061.
43. Mao CA, Li H, Zhang Z, et al. T-box transcription regulator *Tbr2* is essential for the formation and maintenance of Opn4/melanopsin-expressing intrinsically photosensitive retinal ganglion cells. *J Neurosci*. 2014;34(39):13083–13095.
44. Cherry TJ, Trimarchi JM, Stadler MB, Cepko CL. Development and diversification of retinal amacrine interneurons at single cell resolution. *Proc Natl Acad Sci USA*. 2009;106(23):9495–9500.
45. Roesch K, Jadhav AP, Trimarchi JM, et al. The transcriptome of retinal Müller glial cells. *J Comp Neurol*. 2008;509(2):225–238.
46. Stalmans I, Ng YS, Rohan R, et al. Arteriolar and venular patterning in retinas of mice selectively expressing VEGF isoforms. *J Clin Invest*. 2002;109(3):327–336.
47. Dorrell MI, Aguilar E, Friedlander M. Retinal vascular development is mediated by endothelial filopodia, a preexisting astrocytic template and specific R-cadherin adhesion. *Invest Ophthalmol Vis Sci*. 2002;43(11):3500–3510.
48. Edwards MM, McLeod DS, Li R, et al. The deletion of *Math5* disrupts retinal blood vessel and glial development in mice. *Exp Eye Res*. 2012;96(1):147–156.
49. Goto S, Onishi A, Misaki K, et al. Neural retina-specific Aldh1a1 controls dorsal choroidal vascular development via Sox9 expression in retinal pigment epithelial cells. *eLife*. 2018;7:e32358.
50. Wang Y, Smallwood PM, Williams J, Nathans J. A mouse model for kinesin family member 11 (Kif11)-associated familial exudative vitreoretinopathy. *Hum Mol Genet*. 2020;
51. Luhmann UF, Lin J, Acar N, et al. Role of the Norrie disease pseudoglioma gene in sprouting angiogenesis during development of the retinal vasculature. *Invest Ophthalmol Vis Sci*. 2005;46(9):3372–3382.
52. Ye X, Wang Y, Cahill H, et al. Norrin, frizzled-4, and Lrp5 signaling in endothelial cells controls a genetic program for retinal vascularization. *Cell*. 2009;139(2):285–298.
53. Junge HJ, Yang S, Burton JB, et al. TSPAN12 regulates retinal vascular development by promoting Norrin- but not Wnt-induced FZD4/β-catenin signaling. *Cell*. 2009;139(2):299–311.
54. Ye X, Wang Y, Nathans J. The Norrin/Frizzled4 signaling pathway in retinal vascular development and disease. *Trends Mol Med*. 2010;16(9):417–425.
55. Collin RW, Nikopoulos K, Dona M, et al. ZNF408 is mutated in familial exudative vitreoretinopathy and is crucial for the development of zebrafish retinal vasculature. *Proc Natl Acad Sci USA*. 2013;110(24):9856–9861.
56. Zimmerli D, Borrelli C, Jauregi-Miguel A, et al. TBX3 acts as tissue-specific component of the Wnt/β-catenin transcriptional complex. *eLife*. 2020;9:e58123.
57. Dhingra S, Shears DJ, Blake V, Stewart H, Patel CK. Advanced bilateral persistent fetal vasculature associated with a novel mutation in the Norrie gene. *Br J Ophthalmol*. 2006;90(10):1324–1325.
58. Payabvash S, Anderson JS, Nascene DR. Bilateral persistent fetal vasculature due to a mutation in the Norrie disease protein gene. *Neuroradiol J*. 2015;28(6):623–627.
59. Pendergast SD, Trese MT, Liu X, Shastry BS. Study of the Norrie disease gene in 2 patients with bilateral persistent hyperplastic primary vitreous. *Arch Ophthalmol*. 1998;116(3):381–382.

Investigative Ophthalmology & Visual Science

60. Robitaille JM, Wallace K, Zheng B, et al. Phenotypic overlap of familial exudative vitreoretinopathy (FEVR) with persistent fetal vasculature (PFV) caused by FZD4 mutations in two distinct pedigrees. *Ophthalmic Genet*. 2009;30(1):23–30.
61. Wu WC, Drenser K, Trese M, Capone A, Dailey W. Retinal phenotype-genotype correlation of pediatric patients expressing mutations in the Norrie disease gene. *Arch Ophthalmol*. 2007;125(2):225–230.
62. Perelli RM, O'Sullivan ML, Zarnick S, Kay JN. Environmental oxygen regulates astrocyte proliferation to guide angiogenesis during retinal development. *Development*. 2021;148(9):dev199418.
63. Sabri K, Ells AL, Lee EY, Dutta S, Vinekar A. Retinopathy of prematurity: A global perspective and recent developments. *Pediatrics*. 2022;150(3):e2021053924.
64. Fevereiro-Martins M, Marques-Neves C, Guimarães H, Bicho M. Retinopathy of prematurity: A review of pathophysiology and signaling pathways. *Surv Ophthalmol*. 2023;68(2):175–210.
65. Wang Z, Liu CH, Huang S, Chen J. Wnt signaling in vascular eye diseases. *Prog Retin Eye Res*. 2019;70:110–133.
66. Biswas S, Cottarelli A, Agalliu D. Neuronal and glial regulation of CNS angiogenesis and barriergenesis. *Development*. 2020;147(9):dev182279.
67. D'Souza S, Lang RA. Retinal ganglion cell interactions shape the developing mammalian visual system. *Development*. 2020;147(23):dev196535.
68. Mi H, Haeberle H, Barres BA. Induction of astrocyte differentiation by endothelial cells. *J Neurosci*. 2001;21(5):1538–1547.
69. Fruttiger M, Calver AR, Krüger WH, et al. PDGF mediates a neuron-astrocyte interaction in the developing retina. *Neuron*. 1996;17(6):1117–1131.
70. Miyawaki T, Uemura A, Dezawa M, et al. Tlx, an orphan nuclear receptor, regulates cell numbers and astrocyte development in the developing retina. *J Neurosci*. 2004;24(37):8124–8134.
71. Uemura A, Kusuhara S, Wiegand SJ, Yu RT, Nishikawa S. Tlx acts as a proangiogenic switch by regulating extracellular assembly of fibronectin matrices in retinal astrocytes. *J Clin Invest*. 2006;116(2):369–377.
72. Fruttiger M. Development of the retinal vasculature. *Angiogenesis*. 2007;10(2):77–88.
73. Jiang B, Liou GI, Behzadian MA, Caldwell RB. Astrocytes modulate retinal vasculogenesis: Effects on fibronectin expression. *J Cell Sci*. 1994;107(pt 9):2499–2508.
74. Jiang B, Bezhadian MA, Caldwell RB. Astrocytes modulate retinal vasculogenesis: Effects on endothelial cell differentiation. *Glia*. 1995;15(1):1–10.
75. Rattner A, Williams J, Nathans J. Roles of HIFs and VEGF in angiogenesis in the retina and brain. *J Clin Invest*. 2019;130:3807–3820.
76. Stone J, Itin A, Alon T, et al. Development of retinal vasculature is mediated by hypoxia-induced vascular endothelial growth factor (VEGF) expression by neuroglia. *J Neurosci*. 1995;15(7 pt 1):4738–4747.
77. Zhang Y, Stone J. Role of astrocytes in the control of developing retinal vessels. *Invest Ophthalmol Vis Sci*. 1997;38(9):1653–1666.
78. Weiner GA, Shah SH, Angelopoulos CM, et al. Cholinergic neural activity directs retinal layer-specific angiogenesis and blood retinal barrier formation. *Nat Commun*. 2019;10(1):2477.
79. Usui Y, Westenskow PD, Kurihara T, et al. Neurovascular crosstalk between interneurons and capillaries is required for vision. *J Clin Invest*. 2015;125(6):2335–2346.
80. Lyu P, Hoang T, Santiago CP, et al. Gene regulatory networks controlling temporal patterning, neurogenesis, and cell-fate specification in mammalian retina. *Cell Rep*. 2021;37(7):109994.

Supplementary Material

Supplementary Video S1. Wild-type (WT) flat mount retina immunostained with anti-GFP (green) and astrocyte precursor marker, Pax2 (red), shows no overlap in 3D rendered confocal image.

Supplementary Video S2. Transgenic *tbx3*$^{GR/+}$ expresses GFP in astrocyte precursor cells marked by Pax2 in this 3D rendered confocal image.

Supplementary Video S3. Side-by-side comparison of wild-type (WT) and conditional knockout (cKO) retinas at P26.

Supplementary Video S4. Stereotypical tri-layered retinal vascular plexus in wild-type dorsal retina at P26 in 3D rendered confocal image.

Supplementary Video S5. Abnormal bi-layered retinal plexus in *Tbx3* conditional knockout dorsal retina at P26 in 3D rendered confocal image.

Investigative Ophthalmology & Visual Science